

Rothamsted Repository Download

A - Papers appearing in refereed journals

Kuo, P., Tock, A. J., Liu, X., Topp, S. D., Zhong, Z., Henderson, I. R. and Lambing, C. 2025. Histone variant H2A.W7 represses meiotic crossover formation in Arabidopsis heterochromatin. *Proceedings of the National Academy of Sciences*. 122 (22), p. e2414166122.
<https://doi.org/10.1073/pnas.2414166122>

The publisher's version can be accessed at:

- <https://doi.org/10.1073/pnas.2414166122>
- https://www.pnas.org/doi/10.1073/pnas.2414166122?url_ver=Z39.88-2003&rfr_id=ori%3Arid%3Acrossref.org&rfr_dat=cr_pub++0pubmed

The output can be accessed at: <https://repository.rothamsted.ac.uk/item/993w7/histone-variant-h2a-w7-represses-meiotic-crossover-formation-in-arabidopsis-heterochromatin>.

© 29 May 2025, Please contact library@rothamsted.ac.uk for copyright queries.



Histone variant H2A.W7 represses meiotic crossover formation in *Arabidopsis* heterochromatin

Pallas Kuo^{a,b}, Andrew J. Tock^b, Xuexia Liu^c, Stephanie D. Topp^b, Zhenhui Zhong^c, Ian R. Henderson^{b,1}, and Christophe Lambing^{a,b,1}

Edited by James Birchler, University of Missouri, Columbia, MO; received July 15, 2024; accepted February 28, 2025

In eukaryotic genomes, DNA is packaged into nucleosomes to form chromatin. The incorporation of canonical or variant histones into nucleosomes confers different properties and influences chromatin structure to regulate cellular processes, including recombination. During meiosis, DNA double-strand breaks (DSBs) are formed and repaired as interhomolog crossovers. Nucleosome occupancy is generally associated with low crossover frequency, but it remains unclear which histone variants are involved in this process. In *Arabidopsis*, three variants of H2A coexist: H2A.X, H2A.Z, and H2A.W. Here, we show that H2A.W7 has a suppressive role on meiotic recombination. Genome-wide mapping of the crossover landscape revealed increased centromere-proximal recombination in *h2a.w7*. Moreover, H2A.W7 can be recruited to the *3a* crossover hotspot via 21–24-nucleotide siRNAs during RNA-directed DNA methylation, causing increased nucleosome occupancy and decreased crossover frequency. Cytological analysis reveals that H2A.W7 restricts heterochromatin clustering during meiosis, which can form a mechanism to limit interhomolog recombination. Conversely, the linker histone H1, of which its loading is known to be restricted by H2A.W, promotes heterochromatin clustering and crossover on a heterochromatic genetic interval. Our study reveals a role for H2A.W7 in repressing crossover formation in *Arabidopsis*.

meiosis | crossover | H2A.W | nucleosomes | epigenetics

Meiosis is a specialized cell division taking place in germ cells of sexually reproducing eukaryotes. It is characterized by one round of DNA replication, followed by two rounds of chromosome segregation, resulting in the formation of haploid gametes (1). At the start of meiosis, a large number of DNA double-strand breaks (DSBs) are formed by the topoisomerase-like complex SPO11-MTOPVib (2, 3). DSBs are processed to form single-strand overhang DNA (ssDNA), onto which the recombinases RAD51 and DMC1 are recruited (4). DMC1 promotes the invasion of ssDNA into the homologous chromosomes for repair (5–7). Most heteroduplex DNA structures eventually dissociate and the ssDNA anneals back to their sister chromatid, while a subset of heteroduplex DNA structures further mature into reciprocal crossovers. Crossovers lead to exchange of genetic information between homologous chromosomes and contribute to genetic diversity (1).

Meiotic recombination is not randomly distributed along chromosomes, and DSBs and crossovers are enriched within kilobase-scale hotspots, whose locations are determined by genetic and epigenetic factors (8, 9). At the genome scale, *Arabidopsis* crossovers are frequent in the chromosome arms, where chromatin is more accessible (10–12). Crossovers are generally suppressed in the pericentromeric heterochromatic regions, which are enriched in DNA methylation, H3K9me₂, and transposons, although pericentromeric hotspots can be found embedded in the heterochromatin (10–12). *Arabidopsis* mutant lines for the DNA methyltransferase *CMT3* involved in non-CG DNA methylation and histone H3K9 methyltransferases *SUVH4/5/6* show an elevation of crossovers in the pericentromeric heterochromatin (11). In contrast, pericentromeric crossover frequency is reduced in the DNA methyltransferase *Arabidopsis* mutant *met1*, in which DNA methylation in CG context is lost (13). These observations demonstrate that meiotic recombination is regulated by epigenetic information.

In eukaryotes, genomic DNA is packaged into chromatin, which is the substrate for transcription, DNA replication, repair, and recombination. Within chromatin, nucleosomes contain two copies of each of the core histone subunits H2A, H2B, H3, and H4 (14). The N-terminal region of histones are flexible tails that extend away from nucleosomal DNA and influence gene expression and chromatin compaction (14). The histone C-terminal region forms a histone fold domain that creates a complementary interface that allows histone heterodimerization between H2A with H2B, and H3 with H4, and the histone octamer (15, 16). Each pair of dimers in the histone core contributes to the dynamic forces that maintain nucleosome structure (16). The core histones have also

Significance

Meiotic recombination is an evolutionary-conserved process that shapes genetic variation in most eukaryotes. DNA is packaged into nucleosomes, and high levels of nucleosome occupancy suppress recombination. This study reveals that H2A.W7, a histone variant of the H2A family, suppresses recombination in heterochromatin. Genome-wide analysis showed that H2A.W7 associates with transposons containing high level of DNA double-strand breaks (DSBs), which are the precursors for recombination. Artificial deposition of H2A.W7 at a recombination hotspot reduces recombination. Our study provides insights into the molecular mechanisms that influence the meiotic recombination landscape.

Author affiliations: ^aDepartment of Plant Sciences, Rothamsted Research, Harpenden AL5 2JQ, United Kingdom; ^bDepartment of Plant Sciences, University of Cambridge, Cambridge CB2 3EA, United Kingdom; and ^cMinistry of Education Key Laboratory for Bio-Resource and Eco-Environment, College of Life Sciences, State Key Laboratory of Hydraulics and Mountain River Engineering, Sichuan University, Chengdu 610064, China

Author contributions: P.K., I.R.H., and C.L. designed research; P.K., S.D.T., and C.L. performed research; P.K., A.J.T., X.L., Z.Z., I.R.H., and C.L. analyzed data; and P.K., I.R.H., and C.L. wrote the paper.

The authors declare no competing interest.

This article is a PNAS Direct Submission.

Copyright © 2025 the Author(s). Published by PNAS. This open access article is distributed under Creative Commons Attribution-NonCommercial-NoDerivatives License 4.0 (CC BY-NC-ND).

¹To whom correspondence may be addressed. Email: irh25@cam.ac.uk or christophe.lambing@rothamsted.ac.uk.

This article contains supporting information online at <https://www.pnas.org/lookup/suppl/doi:10.1073/pnas.2414166122/-/DCSupplemental>.

Published May 29, 2025.

diversified via gene duplication and acquisition of novel functions and can be divided into canonical histones and variant histones. Some histone variants, such as H2A.Z and centromeric histone H3 (CENH3) are incorporated into specific genomic locations, whereas other variants, such as human H2A.Bbd and mouse H2A.Lap1, show cell- or tissue-specific expression (14, 17).

In *Arabidopsis*, the histone H2A superfamily is composed of canonical H2A and three groups of histone variants, namely H2A.X, H2A.Z, and H2A.W (18, 19). Thermodynamic assays showed that nucleosomes containing H2A.Z9 are less stable than nucleosomes containing H2A.W6, H2A.X3, or H2A.I3 (20). In the H2A family, *H2A.W* genes evolved in vascular plants (21), and in *Arabidopsis*, there are three H2A.W orthologs, *H2A.W6*, *H2A.W7*, and *H2A.W12*, which are defined by the presence of a conserved SPKK motif in the C-terminal tail (18, 22). H2A.W proteins are enriched in heterochromatin and on transposons (22). In vitro studies showed that the SPKK motif of H2A.W condenses nucleosome arrays (20, 22). Functional diversification between *H2A.W* genes is apparent, as H2A.W7 is distinct from H2A.W6 or H2A.W12, due to its SQ motif in its C-terminal tail that can be phosphorylated by ATM in response to gamma irradiation and exposure to the genotoxic agents bleomycin and zeocin (23, 24). H2A.X also possesses an SQ motif in the C-terminal tail (23). H2A.W7 and H2A.X are both implicated in somatic DNA damage response (DDR) (23). However, the role of H2A.X and H2A.W in meiotic DNA repair has not yet been investigated.

In this study, the role of the histone variant H2A.W on meiotic crossover recombination was investigated in *Arabidopsis*. Analyses of ChIP-sequencing profile of H2A.W6 and H2A.W7, the two most expressed H2A.W proteins, revealed that H2A.W7 is associated with DNA transposons containing high level of SPO11-1-oligonucleotides. Through genetic analyses, we demonstrate that H2A.W7 has a suppressive role on crossover formation within the pericentromeric heterochromatin. Cytological investigation of meiotic chromatin reveals that H2A.W7 limits heterochromatin clustering. In *h2a.w6-2 h2a.w7*, *h2a.w7 h2a.w12*, and *h2a.w6-2 h2a.w7 h2a.w12* mutants, recombination frequency within the pericentromeric heterochromatin genetic interval *CEN3* is less than in *h2a.w7*. We propose this reflects the progressive replacement of H2A.W7 with other histone marks and this process can vary between regions along the genome. A phospho-mutant line of H2A.W7 lacking the SQ motif, and *h2a.x*, have no effect on crossover rate or meiotic DNA repair. Expression of 21-24-nucleotide siRNAs and RNA-directed DNA methylation promote deposition of H2A.W7 at the *3a* crossover hotspot, and the removal of H2A.W7 in this line reduces nucleosome occupancy and partially restores recombination frequency. Altogether, we identify H2A.W7 as a factor that suppresses meiotic crossover in *Arabidopsis* heterochromatin.

Results

H2A.W7 Marks a Subset of Transposons that Associates with SPO11-1-Oligonucleotide Hotspots. To examine the presence of H2A.W6 and H2A.W7 during meiosis, we coimmunostained H2A.W6 or H2A.W7 with ASY1, which marks chromosome axis during early prophase I (25), while chromatin was stained by DAPI. The intensity of DAPI staining reflects the abundance of DNA within a defined chromosomal area and was used to compare the level of DNA organization between chromosomal regions. For example, the chromocenters have significantly higher DAPI staining intensity compared to the rest of the chromosomes, which reflect their higher order of chromatin organization and represent heterochromatin regions (*SI Appendix, Fig. S1 and Table S1*) (13). Our results show that both H2A.W6 and H2A.W7

immunostaining signals are localized on the DAPI-dense regions of the chromatin during meiosis (Fig. 1A).

Comparison of the genome-wide profile of H2A.W6 and H2A.W7 ChIP-sequencing (ChIP-seq) (23) with SPO11-1-oligonucleotide sequencing (10), and crossovers mapped by sequencing Columbia-0 (Col) × Landsberg *erecta* (Ler) F₂ plants (26), revealed that H2A.W6 and H2A.W7 are enriched in the heterochromatic regions consistent with our cytological observations (Fig. 1A and B). These regions are depleted for SPO11-1-oligonucleotides and crossovers at the megabase scale (Fig. 1B). To study H2A.W localization at higher resolution, we used PeakRanger suite and identified 18,168 H2A.W6 peaks and 22,831 H2A.W7 peaks genome-wide. H2A.W6 and H2A.W7 peaks were defined as regions of ChIP-seq enrichment over input DNA [$P < 0.001$ and false discovery rate (FDR) < 0.01]. We then analyzed the profile of SPO11-1-oligos over the H2A.W6 or H2A.W7 peaks, and over 10,000 sets of randomly positioned loci with the same width distribution as the H2A.W6 or H2A.W7 peaks (Fig. 1C). We found that SPO11-1-oligos are depleted within H2A.W6 peaks and H2A.W7 peaks, consistent with nucleosomes suppressing SPO11-1-oligos (10). SPO11-1 oligos are also suppressed in adjacent regions of H2A.W6 peaks. In contrast, SPO11-1 oligos are comparatively enriched in the regions immediately adjacent to H2A.W7 peaks, compared to random loci (Fig. 1C). To illustrate this, we show a representative region on chromosome 3 containing SPO11-1-oligos enriched within a *hAT* transposon (Fig. 1D). H2A.W7 peaks can be detected on the edges of the transposon in regions depleted for SPO11-1 oligos, but immediately adjacent to the SPO11-1 oligo-enriched region (Fig. 1D).

To assess H2A.W6 and H2A.W7 in relation to SPO11-1-oligos and transposons in more detail, we divided peaks into four categories: i) H2A.W6 peaks overlapping H2A.W7, ii) H2A.W6 peaks not overlapping H2A.W7, iii) H2A.W7 peaks overlapping H2A.W6, and iv) H2A.W7 peaks not overlapping H2A.W6 (Fig. 1E). For each group, we evaluated overlaps with different transposon families (*SI Appendix, Table S2*), SPO11-1-oligos (10) and nucleosomes (10). We performed permutation tests using 10,000 sets of randomly positioned loci with the same width distributions as H2A.W6 or H2A.W7 peaks and across the length of chromosomes to calculate P -values denoting the significance of overlaps. This revealed that H2A.W6 peaks not containing H2A.W7 were more likely overlapping RNA transposon families, and less likely overlapping DNA transposon families than expected by chance, whereas H2A.W7 peaks without H2A.W6 were more likely overlapping DNA transposon families (Permutation test, $P < 10^{-4}$) (Fig. 1E and *SI Appendix, Table S3*). SPO11-1-oligos were more likely associated with H2A.W7 peaks not containing H2A.W6 than expected by chance, while they negative associated with the other three categories which contains H2A.W6 peaks (Permutation test, $P < 10^{-4}$) (Fig. 1E and *SI Appendix, Table S3*). Overall, our analyses reveal that H2A.W6 and H2A.W7 are differentially associated with transposon families. H2A.W7 peaks not containing H2A.W6 associated with transposons that correlate with high level of SPO11-1-oligos. We noted that H2A.W7 does not overlap SPO11-1 oligos in this subclass of transposons. Instead, high levels of H2A.W7 occurred in the flanking regions of SPO11-1-oligo.

H2A.W7 Suppresses Pericentromeric Meiotic Recombination. To evaluate the role of each of the H2A.Ws in meiotic recombination, we crossed individual mutant lines of *H2A.W6*, *H2A.W7*, and *H2A.W12* with fluorescent-tagged lines (FTLs) (27). *CEN3* is an FTL interval that spans the pericentromere heterochromatin of chromosome 3 and is defined by two transgenes (Fig. 2A) (28). Each transgene contains a pollen-specific promoter (*LAT52*) that expresses a different color of fluorescent protein (27). In

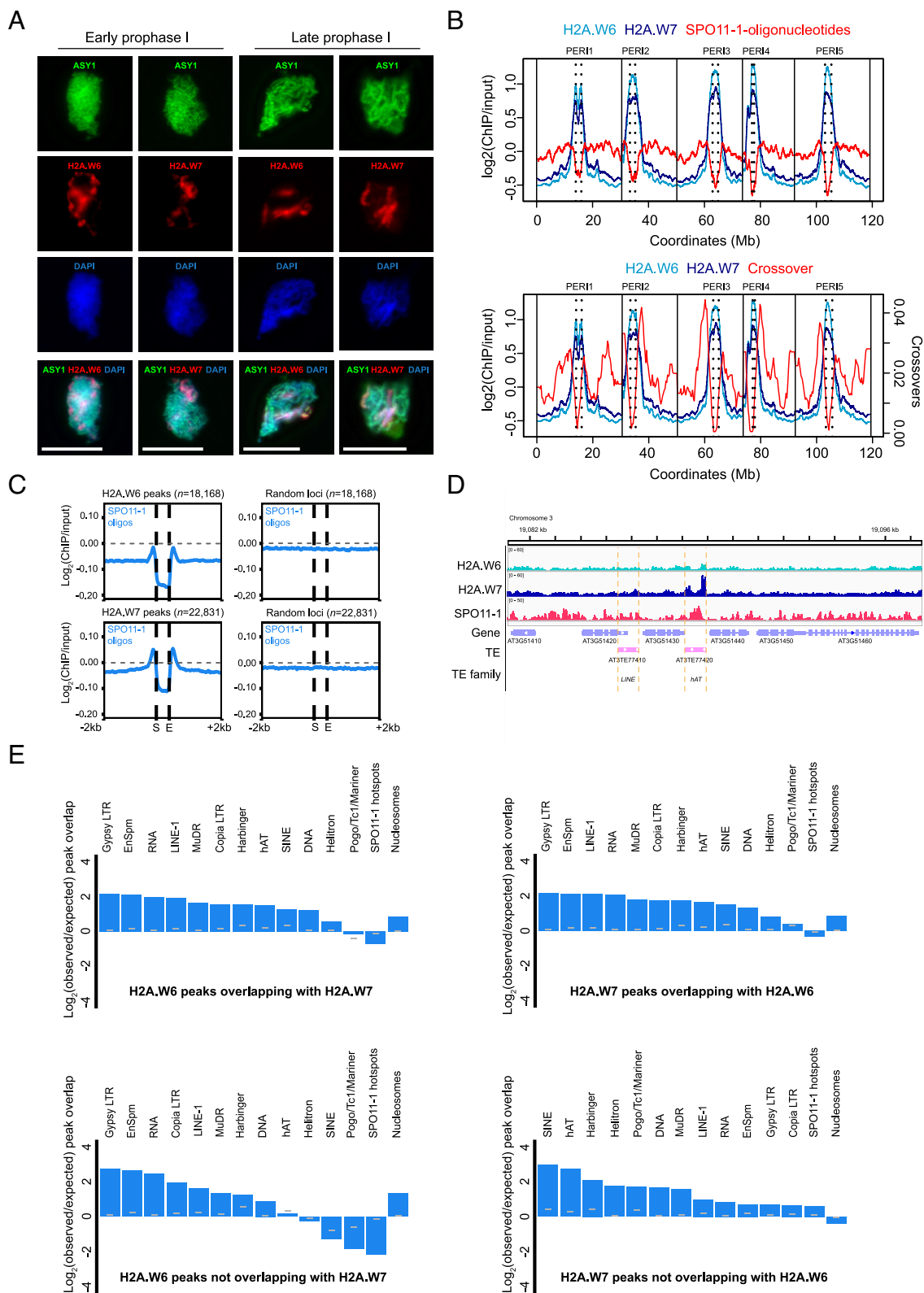


Fig. 1. H2A.W6 and H2A.W7 localization on the chromatin. (A) Immunolocalization of H2A.W6 and H2A.W7 with ASY1 in prophase I. Chromatin is stained with DAPI. (Scale bar, 10 μm .) (B) Profiles of H2A.W6, H2A.W7 [$\log_2(\text{ChIP}/\text{input})$], and SPO11-1-oligonucleotides [$\log_2(\text{oligos}/\text{gDNA})$] in 10-kb cumulative windows along the chromosomes. Crossover frequency is presented in 300-kb cumulative windows. Vertical dotted lines represent the pericentromeres (PERI). (C) Mean coverage of SPO11-1-oligos [$\log_2(\text{oligos}/\text{gDNA})$] within H2A.W6 or H2A.W7 peaks (vertical dashed lines) and 2-kb flanking regions. "S" and "E" represent the start and end of the peaks, respectively. Horizontal dashed lines represent 0-value. (D) A representative region from chromosome 3 showing H2A.W6, H2A.W7, SPO11-1-oligo profiles over genes and transposons. Orange dashed lines delineate an RNA LINE element and a DNA hAT element. Note that hAT contains H2A.W7 and SPO11-1-oligo. (E) Bar graphs showing permutation test derived $\log_2(\text{observed/expected})$ overlap of the genome-wide H2A.W6 and H2A.W7 peaks with the indicated transposon families, SPO11-1-oligonucleotides and nucleosomes. Horizontal gray lines represent the significant threshold of $\alpha = 0.05$.

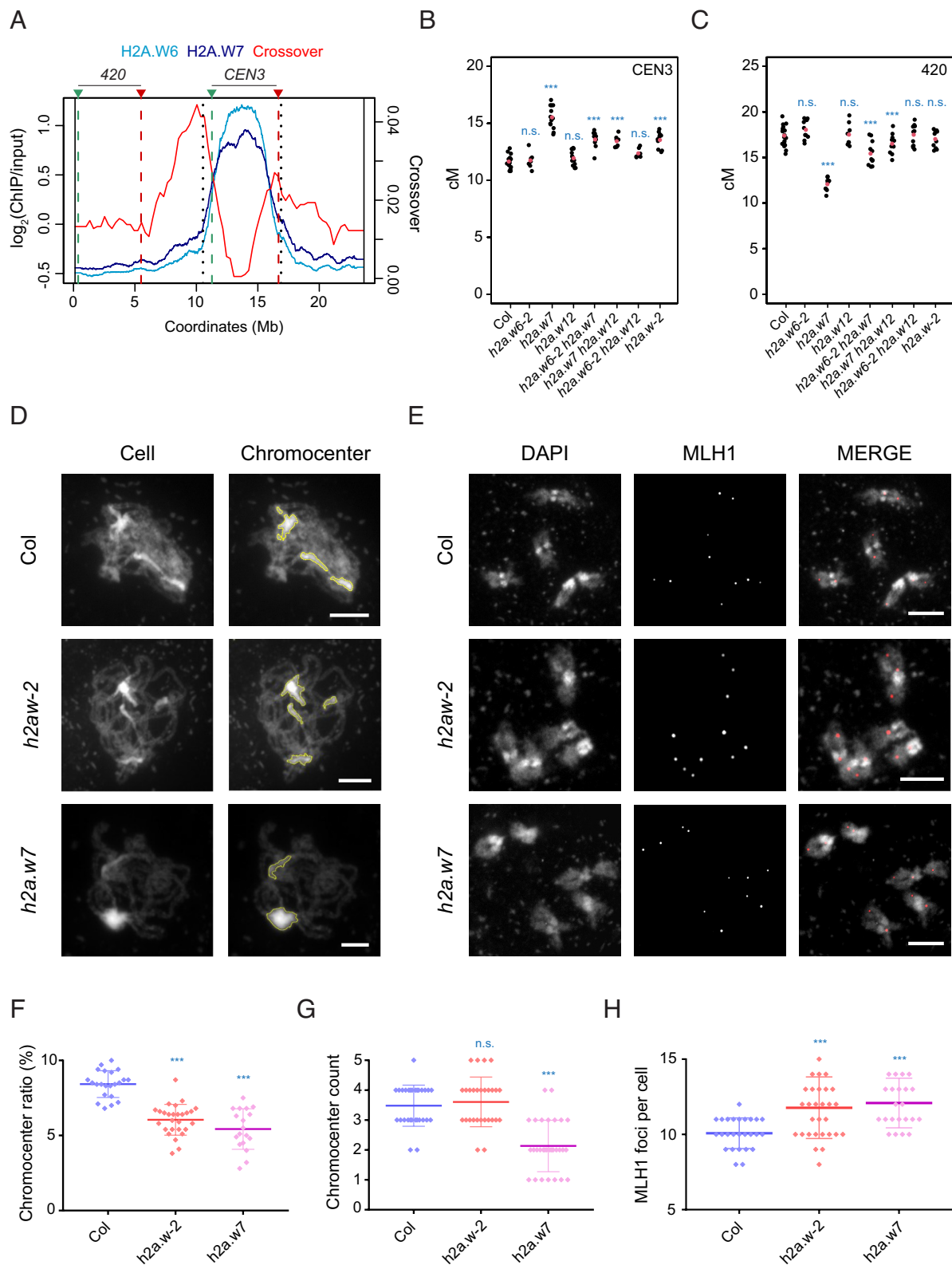


Fig. 2. H2A.W7 influences meiotic recombination and chromatin organization. (A) Profiles of crossover frequency in 300-kb cumulative windows and H2A.W6 and H2A.W7 [$\log_2(\text{ChIP/input})$] in 10-kb cumulative windows along chromosome 3. Vertical dotted lines represent the PERI. Green and red dashed lines delineate the genetic intervals 420 and CEN3. (B and C) Crossover frequency (cM) within CEN3 (B) and 420 (C) intervals in the respective genotypes. Black points represent individual measurements and red points represent mean values. (D) Chromosome spreads of meiotic nuclei at pachytene stage in wild type (Col), *h2a.w7*, and *h2a.w-2*. Chromatin is stained with DAPI and chromocenter areas are defined as regions with higher intensity threshold of DAPI signal. (E) Immunostaining of MLH1 (white/red) on meiotic nuclei at diakinesis stage in wild type (Col), *h2a.w7*, and *h2a.w-2*. Chromatin is stained with DAPI (white). (F) Measurements of percentage chromocenter area/total chromatin area in wild type (Col), *h2a.w7*, and *h2a.w-2*. The mean value and SE of the means are shown. (G) Quantification of chromocenters in wild type (Col), *h2a.w7*, and *h2a.w-2*. Mean value and SE of the means are shown. (H) Quantification of MLH1 foci in wild type (Col), *h2a.w7*, and *h2a.w-2*. Mean value and SE of the means are shown. "n.s." is abbreviated from no significance, $***P < 0.01$. (Scale bar, 10 μm .)

hemizygous plants, when a crossover forms between the two transgenes, it changes patterns of fluorescence inheritance in the pollen (29). Crossover frequency within *CEN3* was 11.6 cM in wild type, and no significant change was observed in *h2a.w6-2* (GLM, $P = 0.286$), or *h2a.w12* (GLM, $P = 0.198$). However, in *h2a.w7*, *CEN3* crossover frequency was increased by a third to 15.5 cM (GLM, $P = 1.2 \times 10^{-83}$) (Fig. 2B and SI Appendix, Table S4), implicating H2A.W7 in mediating pericentromeric repression of crossover frequency.

To test functional redundancy between H2A.W variants, crossover frequency was measured in *CEN3* containing all three combinations of double mutations, and the triple mutant *h2a.w6-2 h2a.w7 h2a.w12* (hereafter *h2a.w-2*). We observed that only double mutant lines that included *h2a.w7*, (*h2a.w6-2 h2a.w7* and *h2a.w7 h2a.w12*) showed significantly increased *CEN3* crossover frequency (Fig. 2B and SI Appendix, Table S4), albeit to a level slightly reduced compared to *h2a.w7*. The *h2a.w-2* triple mutant also showed increased *CEN3* crossover frequency (GLM, $P = 1.5 \times 10^{-22}$), but at an intermediate level between *h2a.w7* and wild type, similar to *h2a.w6-2 h2a.w7* and *h2a.w7 h2a.w12* double mutants (Fig. 2B and SI Appendix, Table S4).

This analysis was repeated using the seed-based FTL 420, which defines a euchromatic subtelomeric interval on the left arm of the chromosome 3 (Fig. 2A) (30). In *h2a.w7*, 420 crossover frequency was decreased by nearly a third from 17.4 cM in wild type to 12.1 cM (GLM, $P = 2.1 \times 10^{-55}$), whereas *h2a.w6* and *h2a.w12* showed no significant change compared to wild type (Fig. 2C and SI Appendix, Table S5). Similar to our observations with *CEN3*, the *h2a.w6-2 h2a.w7* (15.4 cM) and *h2a.w7 h2a.w12* (16.5 cM) double mutants showed a crossover frequency decrease that was intermediate between *h2a.w7* and wild type (Fig. 2C). The *h2a.w-2* triple mutant (17.0 cM) also showed a slight decrease in 420 crossover frequency compared to wild type, although this was not statistically significant (GLM, $P = 0.38$) (Fig. 2C). Except for *h2a.w-2*, the *h2a.w7* mutants that increased *CEN3* recombination phenotype, showed an opposite trend in 420 (Fig. 2B and C and SI Appendix, Tables S4 and S5). These data suggest that the crossover landscape in *h2a.w7* is remodeled on chromosome 3, with distal euchromatic decreases, alongside proximal heterochromatic increases.

H2A.W7 Limits Interchromosomal Heterochromatic Clustering.

We next investigated chromatin structure using DAPI staining on pachytene nuclei in wild type, *h2a.w7*, and *h2a.w-2*. Chromocenter volume and total chromatin volume were measured and the ratio was calculated as a percentage. In wild type, average chromocenter volume was 8.43% per meiocyte, while *h2a.w7* and *h2a.w-2* showed a significantly reduced chromocenter volume, with 5.43 and 6.05%, respectively [Mann–Whitney–Wilcoxon test (MWW), $P = 1.8 \times 10^{-07}$; $P = 3.6 \times 10^{-08}$] (Fig. 2D and F and SI Appendix, Table S6), which demonstrated that heterochromatin organization is reshaped in both mutant lines. To determine whether the association between heterochromatin regions is increased, we assessed the number of chromocenter clusters at pachytene. In wild-type meiocytes, the heterochromatic regions formed an average of 3.5 clusters at pachytene stage, as previously reported (31) (Fig. 2D and G and SI Appendix, Table S7). A similar number of clusters were found in *h2a.w-2* (3.6, MWW, $P = 0.621$). In *h2a.w7*, however, chromocenter cluster count decreased by 40% compared to wild type, with an average of only 2.1 clusters per meiocyte (MWW, $P = 3.7 \times 10^{-07}$), (Fig. 2D and G and SI Appendix, Table S7). Crossover events in *h2a.w7* and *h2a.w-2* were also quantified cytologically via immunostaining of a marker of Class I crossovers MLH1, on male diakinesis meiocytes (32). In wild type, MLH1 foci counts on chromatin had an average of 10.1 per meiocyte. In *h2a.w7* and *h2a.w-2*, the number of MLH1

foci per cell was increased to 12.1 and 11.8, respectively (MWW, $P = 3.4 \times 10^{-05}$; $P = 1.1 \times 10^{-03}$) (Fig. 2E and H and SI Appendix, Table S8). Altogether, these data show that *h2a.w7* and *h2a.w-2* show a different configuration of heterochromatin during meiosis. The reduction in chromocenter ratio and higher chromocenter clustering in *h2a.w7* could facilitate homology recognition and crossover formation in heterochromatin.

Genome-Wide Mapping of Crossovers Reveals Increased Pericentromeric Recombination in *h2a.w7*.

To evaluate the effect of H2A.W7 on crossover distributions, we mapped crossovers using genotyping-by-sequencing (GBS). The Columbia (Col) *h2a.w7* mutation was first introgressed into the Ler accession, and *h2a.w7 CEN3^{+/-}* ColxLer F₁ hybrid lines were generated. We measured *CEN3* crossover frequency and observed a significant elevation in *h2a.w7* ColxLer hybrids when compared to wild-type ColxLer hybrids (GLM, $P = 4.0 \times 10^{-68}$) (Fig. 3A and SI Appendix, Table S9). This indicates that the crossovers gained in heterochromatin in *h2a.w7* are not sensitive to the presence of interhomolog polymorphism. The *h2a.w7* F₁ hybrids were then self-fertilized and 144 F₂ individuals were sequenced and crossovers mapped. Chromosome 5 was excluded in the analysis due to the position of the *h2a.w7* introgression site, which remains Col-0/Col-0 in our introgressed line. The *h2a.w7* GBS crossover data were compared with equivalent F₂ data from 245 wild-type ColxLer hybrids (26). In GBS analysis, crossovers per F₂ individuals were measured as the sum of male and female recombination events, reflecting the result of two meioses. Since female meiocytes have lower crossover numbers than male meiosis (33), total crossover frequency from GBS analysis is expected to be slightly less than from *CEN3* assays where only male meiosis outcome is measured. Consistent with this, crossover frequency within the *CEN3* interval increased from 22.4 cM in wild type to 28.5 cM in *h2a.w7*, while 420 crossover frequency in *h2a.w7* was reduced from 24.5 cM to 21.5 cM, replicating our observations made from FTLs (Figs. 2B and C and 3B).

Genome-wide analysis was performed to determine total crossover number. On average, wild type and *h2a.w7* have 5.8 and 6.0 crossovers per F₂ individual (t test, $P = 0.409$), and the numbers of crossovers per chromosome was positively correlated with their physical length (Fig. 3C and SI Appendix, Table S10). To study crossover distributions, we defined the pericentromeres (PERI) as in ref. 11. Crossovers were plotted along chromosomes (Fig. 3D). Crossovers were also plotted along the proportional length of all chromosome arms along telomere–centromere axes (Fig. 3E). In *h2a.w7*, crossovers are higher in the PERI and in the euchromatin regions that are directly adjacent to the PERI, while crossovers are reduced in subtelomeric regions (Fig. 3D and E). Certain chromosomes appear to have a greater increase in pericentromeric crossovers than others (SI Appendix, Table S11). On chromosome 2, the left pericentromeric region gains crossover, while the right region shows decreased crossovers in *h2a.w7* (Fig. 3D and SI Appendix, Table S11). A similar crossover landscape on chromosome 2 was observed in *cmt3*, which was also reported to have increased crossovers over heterochromatin regions (11). It remains unclear what factors cause these phenotypes, but it is thought that structural variation and the proximity of a nucleolar organizing region on chromosome 2 could have a role. Although some region-specific effects are observed, the proportion of crossovers over the PERI is increased genome-wide (Fig. 3E). We applied a Benjamini–Hochberg (BH) multiple-testing-corrected P -values and confirmed that the increase in crossovers within PERI in *h2a.w7* was statistically significant (SI Appendix, Fig. S2). Finally, the presence of crossovers within centromeric regions was evaluated using the

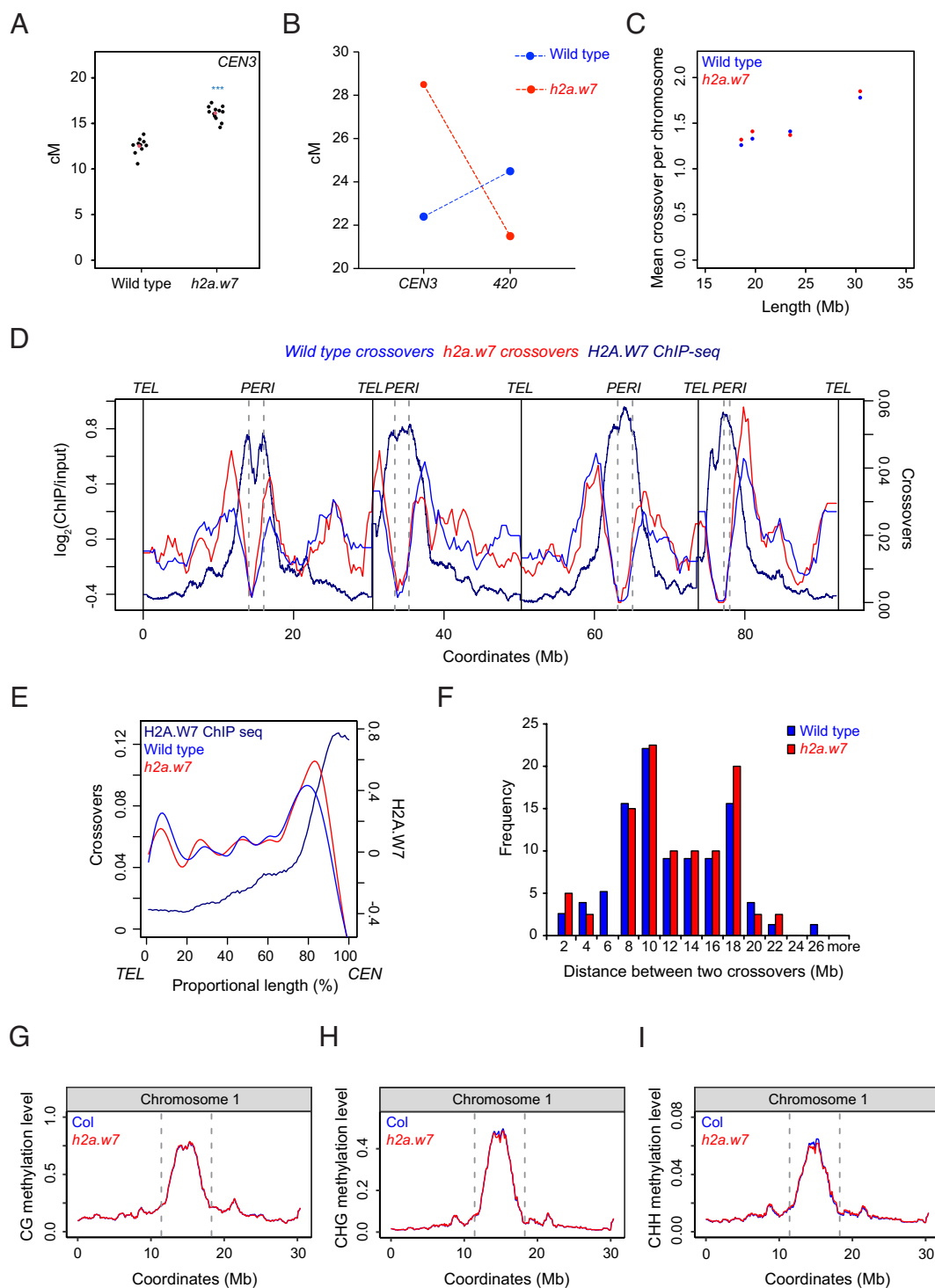


Fig. 3. H2A.W7 suppresses crossover frequency in the heterochromatic pericentromeric regions. (A) Crossover frequency (cM) within the *CEN3* interval in wild type and *h2a.w7* ColxLer F₁ hybrids. Black points represent individual measurements and red points represent mean values. (B) Crossover frequency within *CEN3* and 420 intervals in wild type and *h2a.w7* ColxLer F₁ hybrids by genotyping-by-sequencing (GBS). (C) Mean crossover number for the chromosomes 1 to 4 in ColxLer hybrid of wild type and *h2a.w7*. (D) Crossover distribution along the chromosomes 1 to 4 using 300-kb adjacent windows in ColxLer hybrid of wild type and *h2a.w7*. Solid vertical lines represent the telomeres (TEL). Vertical dashed lines represent the PERI. (E) Crossover distribution along a telomere-to-centromere axis in ColxLer hybrid of wild type and *h2a.w7*. (F) Histogram showing frequency of cis-DCO distances in 2-Mb windows for wild type and *h2a.w7* Col/Ler. (G–I) Profile of DNA methylation in CG (G), CHG (H), and CHH (I) contexts on chromosome 1 from Col and *h2a.w7*.

coordinates in (11). No centromeric crossovers were detected in 245 F₂ wild-type plants, while 2 centromeric crossovers were detected in 144 F₂ *h2a.w7* plants. Hence, crossover formation within centromeres remains mostly repressed in *h2a.w7*.

The genome-wide crossover landscape is influenced by crossover interference (34). Crossovers may be identified in the same meicyte

(*cis*), or a different meicyte (*trans*), when using F₂ GBS data. Double crossover events in a *cis* configuration with the genotypes Col-Het-Col and Ler-Het-Ler can be used for crossover interference measurements (SI Appendix, Fig. S3). The distance between these *cis* double crossover events was previously used to evaluate the strength of crossover interference between genotypes and was found to be consistent with other

crossover interference assays (26, 35). We observed 77 and 40 *cis* double crossover events in wild type and *h2a.w7*, respectively. The mean distance between *cis* crossovers in wild type (11.2 Mb) and *h2a.w7* (11.7 Mb) were not significantly different (MWW, $P = 0.489$) and not random (MWW, $P = 2.6 \times 10^{-10}$; 8.3×10^{-9}), indicating the action of crossover interference (Fig. 3*F*). To assess whether the change of crossover landscape is associated with a change of DNA methylation, whole genome bisulfite sequencing was performed on the floral buds of Col and *h2a.w7*. The level of DNA methylation in CG and CHG contexts is similar between wild type and *h2a.w7* while the level of CHH methylation showed subtle decreases over the PERI in *h2a.w7* (Fig. 3*G–I* and *SI Appendix*, Fig. S4). Overall, our findings demonstrate that the crossover remodeling from distal regions to centromere-proximal regions, corresponding to regions with low and high H2A.W7 occupancy in wild type, respectively, is likely due to a direct repressive role of H2A.W7 in the heterochromatin and the action of crossover interference.

Effects of H2A.W7, CMT3, H1.1, and H1.2 on Crossover Formation.

Immunoprecipitation of CMT3 coupled with mass spectrometry identified H2A.W7 as an interacting protein (36). Since *cmt3* and *h2a.w7* show some similarities in their genome-wide crossover landscape (11), the genetic interaction was tested between *h2a.w7* and *cmt3* using the *CEN3* FTL. Crossover frequency within *CEN3* was increased in *cmt3 h2a.w7* double mutants compared to wild type (GLM, $P = 1.8 \times 10^{-114}$), but did not increase further compared to either of the single mutants (GLM, $P_{\text{vs } cmt3} = 0.159$; $P_{\text{vs } h2a7} = 0.584$) (Fig. 4*A* and *SI Appendix*, Table S12). RNA-sequencing was also performed on floral buds in *cmt3*, *h2a.w7*, and *cmt3 h2a.w7*, which revealed that only few transposons were affected in each line (*SI Appendix*, Table S13).

A previous study showed that in the absence of H2A.W, the level of the linker histone H1 on pericentromeric heterochromatin increases, as non-CG DNA methylation decreases (37). Conversely, loss of H1 leads to an increase of non-CG DNA methylation in

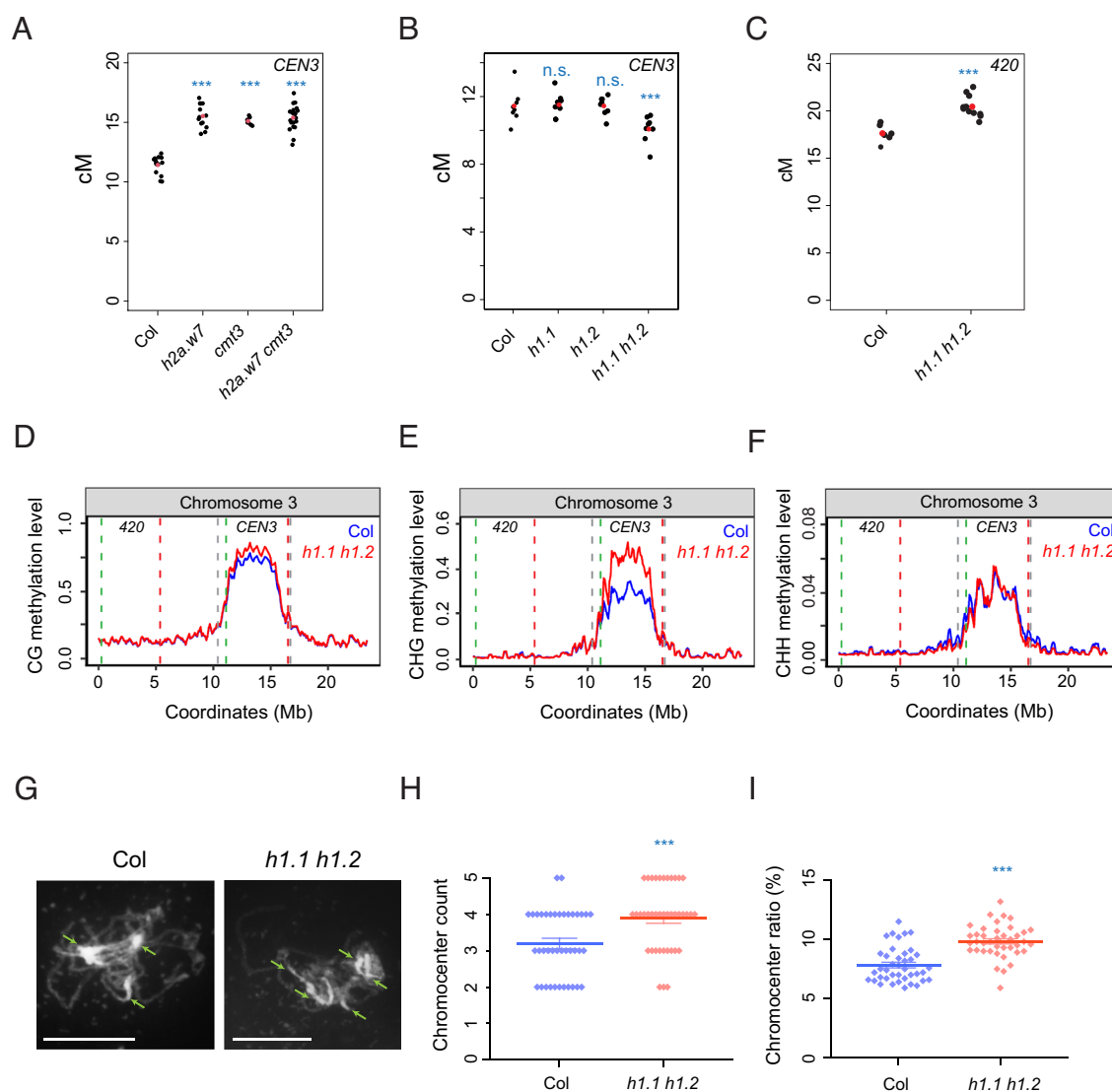


Fig. 4. Analysis of meiotic recombination in *h2a.w7*, *cmt3*, *h1.1*, and *h1.2*. (A) Crossover frequency (cM) within *CEN3* interval in wild type (Col), *h2a.w7*, *cmt3*, and *h2a.w7 cmt3*. Black points represent individual measurements and red points represent mean values. (B and C) Crossover frequency (cM) within *CEN3* (B) and 420 (C) intervals in wild type (Col), *h1.1*, *h1.2*, and *h1.1 h1.2*. Black points represent individual measurements and red points represent mean values. ("n.s." is abbreviated from no significance, *** $P < 0.01$). (D–F) Profile of DNA methylation in CG, (D), CHG (E), and CHH (F) contexts on chromosome 3 from Col and *h1.1 h1.2*. Vertical dashed lines represent the PERI. Red and green dashed lines delineate 420 and *CEN3* genetic intervals. (G) Chromosome spreads of meiotic nuclei at pachytene stage in wild type (Col) and *h1.1 h1.2*. Chromatin is stained with DAPI and chromocenters are indicated by green arrows. (Scale bar, 10 μm .) (H) Quantification of chromocenters in wild type (Col) and *h1.1 h1.2*. Mean value and SE of the means are shown in bars. (I) Measurements of chromocenter percentage in wild type (Col) and *h1.1 h1.2* using the ratio of chromocenter area: total area of chromatin. Mean value and SE of the means are shown in bars. *** $P < 0.01$ (MWW test).

pericentromeric heterochromatin (Fig. 4 D–F) (38). Since non-CG DNA methylation suppresses meiotic recombination (11), we hypothesized that H1 influences meiotic recombination. *H1* is encoded by *H1.1*, *H1.2*, and *H1.3*. *H1.1* and *H1.2* are highly expressed and *H1.3* is only transcriptionally induced in response to abiotic stress (39). Crossover frequency of *h1.1* and *h1.2* were measured in *CEN3* interval and were observed to show a similar level to Col (GLM, $P = 0.911$; $P = 0.811$) (Fig. 4B and *SI Appendix*, Table S14). However, the *h1.1 h1.2* double mutant showed a reduced crossover frequency (GLM, $P = 5.3 \times 10^{-6}$) (Fig. 4B and *SI Appendix*, Table S14). Crossover frequency was also measured within the euchromatic interval 420, and the level of recombination was increased in *h1.1 h1.2* (GLM, $P = 2.6 \times 10^{-6}$) (Fig. 4C and *SI Appendix*, Table S15). Chromosome spreads of meiotic cells show that in *h1.1 h1.2*, chromocenters at pachytene are less clustered (3.9 vs. 3.2; MWW, $P = 1.4 \times 10^{-3}$) and more defined, that often present in elongated shapes (Fig. 4G). Analysis of the chromocenters revealed a 25% increase in chromocenter volume compared to Col (MWW, $P = 2.7 \times 10^{-7}$) (Fig. 4 H and I and *SI Appendix*, Tables S16 and S17). Overall, these indicate that loss of *H1.1* and *H1.2* causes a reduction in chromocenter clustering and is associated with increases in non-CG DNA methylation and crossover frequency reductions in heterochromatin.

H2A.W7 and H2A.X are Dispensable During Meiotic DSB Repair.

H2A.W7 S136 and H2A.X S139 residues are phosphorylated (γ H2A.X) by the ATM kinase in response to DNA damage, and H2A.W7 and H2A.X were shown to act in the same genetic pathway to respond to somatic DNA damage in *Arabidopsis* (23, 24). Since DSBs are formed in large number during meiosis, it is plausible that H2A.W7 and H2A.X have a role in meiotic DNA repair. We therefore tested the role of H2A.X in meiotic recombination. *Arabidopsis* H2A.X is encoded by *H2A.X3* and *H2A.X5*. Coimmunostaining of ASY1 and γ H2A.X on *Arabidopsis* meiotic cells confirmed that γ H2A.X is localized on chromatin, including within the chromocenters (Fig. 5 A and B) (13). Immunostaining of MLH1 was performed on diakinesis nuclei in wild type and a *h2a.x* double mutant (*h2a.x3 h2a.x5*), which showed that the total number of MLH1 foci was not different from wild type (11.2 vs. 10.8; MWW, $P = 0.336$) (Fig. 5 C and D and *SI Appendix*, Table S18). FTL genetic assays were also applied in *h2a.x*. Crossover frequency within *CEN3* and 420 intervals was similar between wild type and *h2a.x* (GLM, $P = 0.157$; $P = 0.935$) (Fig. 5 F and G and *SI Appendix*, Tables S19 and S20), indicating that *H2A.X3* and *H2A.X5* are not essential for meiotic recombination in these regions.

To investigate whether H2A.X and H2A.W7 are involved in meiotic DSB repair, meiotic progression of wild type, *h2a.x*, and *h2a.w7* was cytologically analyzed by DAPI staining of the chromosomes. In wild type, unsynapsed chromosomes enter meiosis before completing synapsis at pachytene. In metaphase I, five bivalents connected by crossovers were observed and balanced chromosome segregations led to two and four pools of chromosomes at dyad and telophase II, respectively (Fig. 5E). In *h2a.x* and *h2a.w7*, chromosomes paired normally at pachytene, five bivalents were observed at metaphase I and balanced chromosome segregation was apparent in meiosis I and meiosis II (Fig. 5E). Chromosome fragmentation, which is an indicator for defects in meiotic DSB repair, was not observed in *h2a.x* or *h2a.w7* mutants.

To test whether H2A.W7 S136 could influence crossover formation, a transgene containing full-length H2A.W7, where the serine residue was replaced by an alanine residue (S136A), was

transformed into *h2a.w7* to mimic the absence of phosphorylation. A wild-type H2A.W7 transgene was also transformed into *h2a.w7* as a control. In both lines, transgenes were expressed under the endogenous H2A.W7 promoter. We observed that *h2a.w7:H2A.W7* *CEN3* crossover frequency was restored to wild-type levels (GLM, $P = 0.104$), and was lower than *h2a.w7* (GLM, $P = 4.6 \times 10^{-116}$) (Fig. 5H and *SI Appendix*, Table S21). This confirms that the H2A.W7 transgene rescues the crossover phenotype of *h2a.w7*. In *h2a.w7:H2A.W7-S136A*, *CEN3* crossover frequency was lower than *h2a.w7* (GLM, $P = 1.6 \times 10^{-118}$), and not significantly different to wild type (GLM, $P = 0.08$), or *h2a.w7:H2A.W7* (GLM, $P = 0.701$) (Fig. 5H and *SI Appendix*, Table S21). Overall, these data indicate that residue S136 of H2A.W7 does not play a role in the control of meiotic recombination.

Recruitment of H2A.W7 by RNA-Directed DNA Methylation Increases Nucleosome Occupancy and Decreases Crossover Frequency at the 3a Recombination Hotspot.

Crossover designation is biased toward specific genomic loci, called crossover hotspots, such as the *3a* locus in the subtelomeric region of chromosome 3 (28). Crossover hotspot activity of *3a* can be silenced in the *HP3* line by expression of homologous inverted repeat hairpins, which produce 21–24-nucleotide siRNAs that direct the RdDM pathway to methylate DNA on the endogenous *3a* sequences (13). To gain further insight into how H2A.W7 suppresses meiotic recombination, *h2a.w7* was studied in combination with *HP3* (13). First, chromatin immunoprecipitation (ChIP) of H2A.W7 was performed on floral buds of Col and *HP3*, followed by qPCR assays on four loci; *HP3-1* and *HP3-2*, which are within *3a*; *Ta2* which acts as a control heterochromatic locus for normalization of Ct values, and *ACTIN7*, as a control for a euchromatic locus (13). Using this assay, a low level of H2A.W7 enrichment was detected over *HP3-1* and *HP3-2* in wild-type Col. In contrast, in the *HP3* line, H2A.W7 is substantially enriched within *HP3-1* (t test, $P = 2.1 \times 10^{-7}$), and *HP3-2* ($P = 1.3 \times 10^{-7}$) (Fig. 6 A and B and *SI Appendix*, Table S22). This indicates that RNA-directed DNA methylation at *3a* creates a chromatin environment favorable for the recruitment of H2A.W7 during crossover silencing.

Bisulfite sequencing showed no detectable DNA methylation within *3a* locus in wild type, while the level of CG and CHG DNA methylation exceeded 50%, and CHH DNA methylation exceeded 10% within the locus in *HP3* transgenic lines. In *HP3 h2a.w7*, the level of DNA methylation is similar to *HP3* (Fig. 6 C and D). We note that the use of unopened floral buds could lead to a limitation in the analysis since floral buds contain a mixture of different cell types. However, the use of unopened floral buds may not skew the methylome analysis as a previous study showed that male meiotic cells have a typical germline methylome (40).

To determine whether H2A.W7 influences *3a* crossover frequency, crossover events that occurred within *3a* were analyzed in Col/Ler F₁ hybrid plants of wild type, *HP3* and *HP3 h2a.w7* via pollen-typing (41). Allele-specific oligonucleotides were used to amplify a series of titrated genomic DNA to determine the proportion of nonrecombinant and recombinant molecules for each genotype. Leaf DNA from hybrid F₁ plants was used as negative control in this assay. *3a* crossover frequency was significantly decreased in *HP3* (14.3 cM/Mb, χ^2 , $P = 3.1 \times 10^{-14}$), compared to wild type (33.5 cM/Mb) (*SI Appendix*, Table S23). In *HP3 h2a.w7*, *3a* crossover frequency was partially restored to 21.7 cM/Mb [χ^2 , $P_{(vs\ HP3)} = 2.5 \times 10^{-7}$; $P_{(v\ WT)} = 2.3 \times 10^{-4}$] (*SI Appendix*, Table S23). To examine the crossover landscape

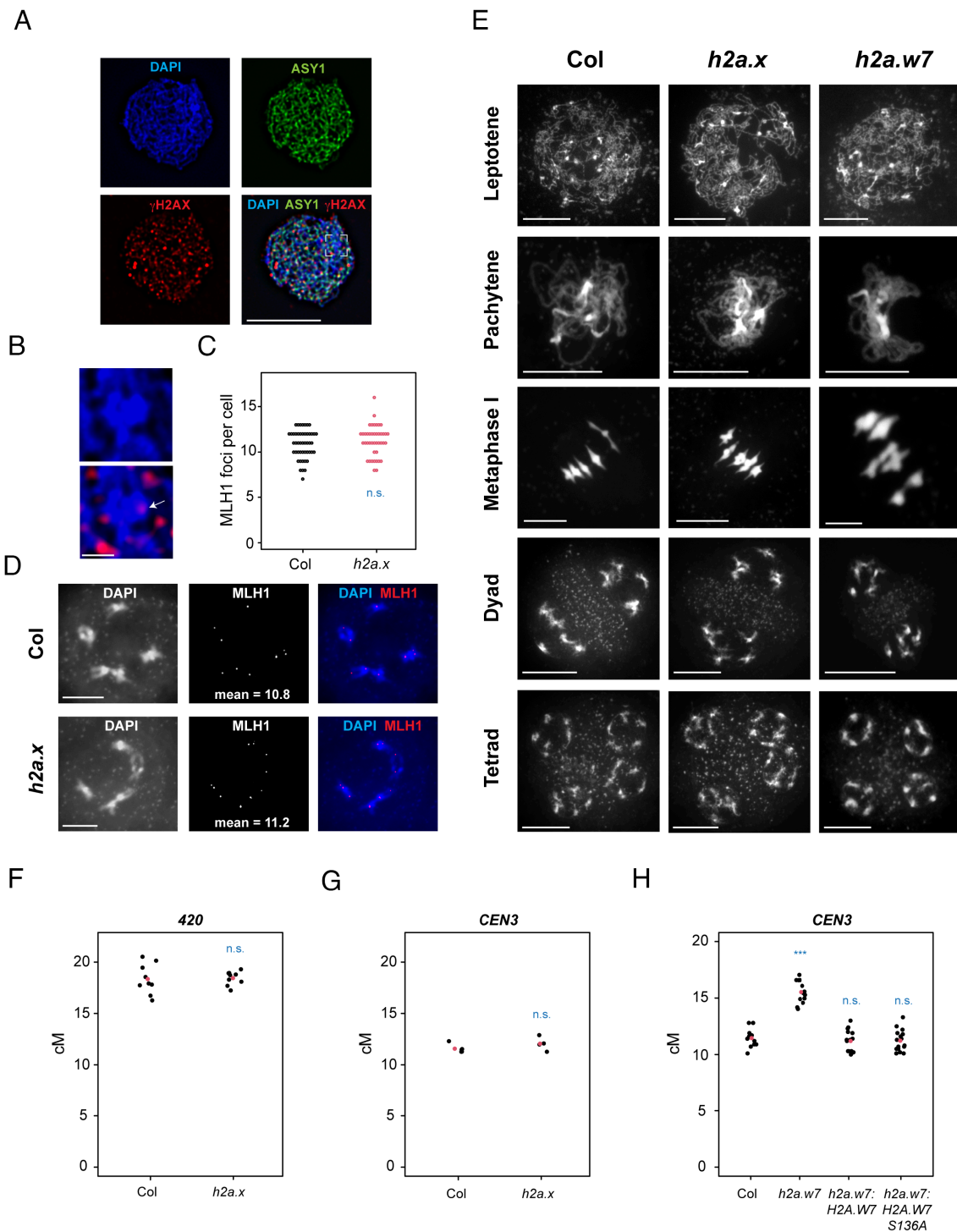


Fig. 5. H2A.W7 and H2A.X are not essential for meiotic DSB repair. (A) Immunocolocalization of ASY1 and γ H2AX on a meiotic nucleus at leptotene stage. Chromatin is stained with DAPI. (Scale bar, 10 μ m.) (B) Zoom-in views of γ H2AX (red) staining on DAPI-stained chromatin (blue). The white arrow shows that γ H2AX foci are observed on chromocenters. (Scale bar, 1 μ m.) (C) Quantification of MLH1 foci in Col and *h2a.x* at diakinesis stage. (D) MLH1 (white/red) immunostaining on meiotic chromosomes at diakinesis stage. Chromatin is stained with DAPI (white/blue). Mean values of MLH1 count are stated on the representative images. (Scale bar, 10 μ m.) (E) Chromosome spread of Col, *h2a.x*, and *h2a.w7* meiocytes at the specified stages. Chromatin is stained with DAPI. (Scale bar, 10 μ m.) (F and G) Crossover frequency (cM) within 420 (F) and CEN3 (G) intervals in Col and *h2a.x*. Black points represent measurements from independent plants, and red points represent mean values. (H) Crossover frequency (cM) within CEN3 interval in the respective genotypes. Black points represent measurements from independent plants, and red points represent mean values. ("n.s." means no significance, *** P < 0.05).

within *3a*, 60 crossover molecules were Sanger sequenced from each genotype, and the crossover locations were identified using single nucleotide polymorphisms (SNPs). In wild type, crossovers are enriched in regions between 634 to 635 kb and 638 to 639.5 kb within the *3a* locus. Both regions lost crossover frequency in *HP3*. In *HP3 h2a.w7*, the crossover frequency in

both regions was at an intermediate level between wild type and *HP3* (Fig. 6E).

According to in vitro assays, H2A.W confers a higher stability to nucleosomes (20). To test whether the loss of H2A.W changes chromatin accessibility, MNase-qPCR, with primers for *HP3-1*, *HP3-2*, *Ta2*, and *ACTIN7* loci, were performed on floral buds of Col, *HP3*,

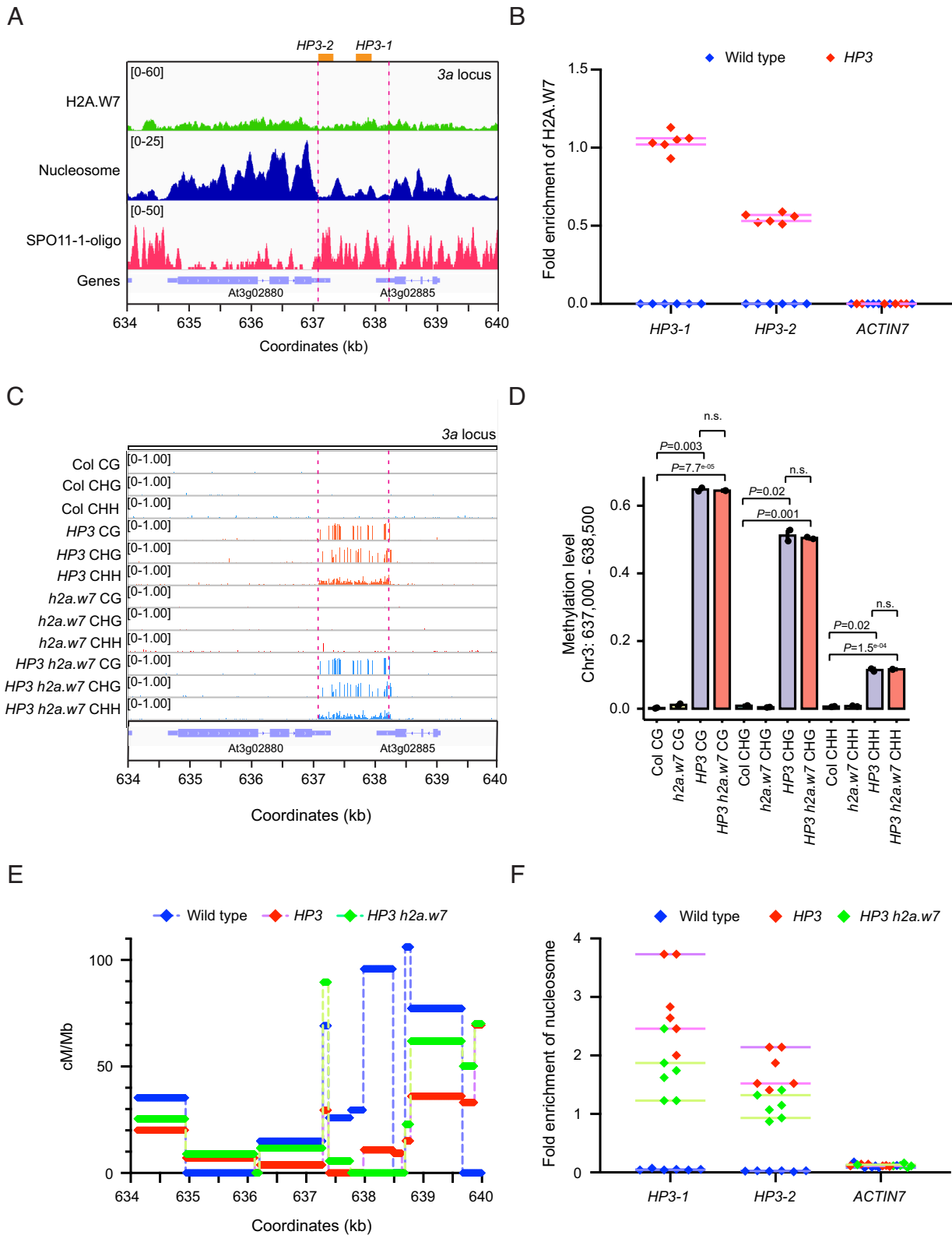


Fig. 6. H2A.W7 suppresses crossover formation on 3a hotspot. (A) Representation of the 3a crossover hotspot locus showing H2A.W7, nucleosomes, SPO11-1-oligonucleotides, and genes. Pink vertical dashed lines represent the region targeted by the HP3 hairpin. Orange boxes represent the regions analyzed by qPCR assay. (B) Fold enrichment of H2A.W7 ChIP on HP3-1, HP3-2, and ACTIN7 relative to Ta2 in Col, HP3, and HP3 h2a.w7. (C) IGV browser view of DNA methylation with the 3a locus in Col, HP3, h2a.w7, and HP3 h2a.w7. Pink horizontal dashed lines represent the region targeted by the HP3 hairpin. (D) The bar graph shows the level of DNA methylation in CG, CHG, and CHH contexts within chromosome 3: 637 to 638.5 kb in Col, HP3, h2a.w7, and HP3 h2a.w7. *t* tests were performed to test for differences between genotypes. "n.s." means not significant. (E) Recombination rate in cM/Mb within the 3a locus in ColxLer hybrid of wild type, HP3 and HP3 h2a.w7. (F) Fold enrichment of nucleosomes on HP3-1, HP3-2, and ACTIN7 relative to Ta2 in Col, HP3, and HP3 h2a.w7.

and HP3 h2a.w7. In HP3 h2a.w7, nucleosome occupancy was reduced by 42.9% and 37.3% in HP3-1 and HP3-2 loci, respectively, compared to HP3 ($P = 3.6 \times 10^{-3}$, 2.0×10^{-3}) (Fig. 6F and SI Appendix,

Table S24). This observation indicates that H2A.W7 increases nucleosome occupancy, and that loss of H2A.W7 creates a more accessible chromatin environment that favors crossover formation.

Discussion

Members of the plant-specific H2A.W family have been reported to show functional diversification in *Arabidopsis* (21–23). Immunolocalization and ChIP-seq data show that H2A.W6 and H2A.W7 overlap at the chromosomal scale. However, the two proteins present distinct localization patterns at the kilobase scale. H2A.W6 peaks significantly overlap RNA transposons that negatively associated with SPO11-1 oligos. In contrast, H2A.W7 peaks overlap DNA transposons. Notably, H2A.W7 peaks without H2A.W6 positively overlap Helitron and Pogo/Tc1/Mariner, which were previously shown to contain SPO11-1-oligo hotspots (10). Our data using the *CEN3* FTL, GBS, and pollen typing show that the deposition of H2A.W7 causes a change in epigenetic environment that disfavors crossover formation. While H2A.W is deposited within the *3a* locus via RdDM, the deposition of H2A.W7 does not appear to affect the level of DNA methylation. Instead, nucleosome occupancy is influenced by H2A.W7. Since nucleosome occupancy is a known antagonizing factor to DSB formation, the recruitment of H2A.W7 could reduce DSB numbers and thus reduce crossover frequency (10). H2A.W7 could also have a role downstream DSB formation by restricting chromocenter clustering, which may limit interhomologous recombination. To determine how and when H2A.W suppresses meiotic recombination and whether H2A.W7 deposition could be influenced by DSB formation, further studies will be required.

Previous studies showed that H2A.W limits the deposition of H1 in the pericentromeric regions while H1 restricts RdDM positioning in the pericentromeric regions (37, 38). Epigenetic homeostasis has been reported in *h2a.w-2* with H2A, H2A.X, and H1 repositioned toward H2A.W loci in pericentromeric heterochromatin (37). The gain of H1 in the pericentromeric regions in *h2a.w2* is associated with a decrease in non-CG DNA methylation on H2A.W peaks in PERI and a gain of non-CG DNA methylation on H2A.W peaks in chromosome arms (37), which is consistent with the gain of recombination frequency we observed in the pericentromeric interval *CEN3* in *h2a.w-2*. Also consistent with this, loss of H1 increases CHG DNA methylation on heterochromatic transposons and decreases CHH DNA methylation on euchromatic transposons (38). This is associated with a redistribution of crossovers from pericentromeric heterochromatin toward the chromosome ends. Similar compensatory effects are expected to occur in single and double mutants of *h2a.w*. FTL analyses using *CEN3* and 420 FTLs reveal a redistribution of meiotic recombination between the two intervals located on the same chromosome and the effects vary between the different combinations of *h2a.w* mutants. This observation is consistent with epigenetic marks being repositioned in the mutants.

Several proteins involved in somatic DNA repair are also expressed during meiosis, but it remains unclear whether their function is similar between the two cell types. H2A.W7 and H2A.X have an SQ motif in the C-terminus that is phosphorylated by ATM in response to DNA damage in somatic cells (23, 24). During DDR, γ H2AX interacts with a BRCA-like protein, XIP, that interacts with RAD51, a recombinase protein that establishes sister chromatid strand invasion in somatic homologous recombination (42). In meiocytes, however, the strand invasion activity of RAD51 is not essential for meiotic DSB repair due to the presence of the meiotic-specific recombinase DMC1 (7, 43). Thus, although H2A.X or H2A.W7 are present during meiosis, their function in DSB repair is not essential.

Overall, our data show that H2A.W7 increases nucleosome occupancy and has a suppressive role on crossover formation in heterochromatin.

Materials and Methods

A detailed description of plant materials, cytological approach, and whole genome bisulfite sequencing is in (SI Appendix, Experimental Procedure).

Plant Materials. *Arabidopsis* plants were propagated in growth chambers under long day conditions at 20 °C.

Crossover Measurement using FTLs. Seed images were captured with a Leica M165 FC microscope and analyzed with CellProfiler. Fluorescence intensity values were determined for each seed and recombination measurement was measured as described (44).

Inflorescences with open flowers were collected and pollen grains were purified as described (29). Fluorescence in each pollen grain was measured using an Accuri C6 (BD Biosciences) flow cytometer and recombination measurement was performed as described (29).

Cytological Approaches. Spreads of meiotic chromosomes were performed using acetic acid-based protocol (45). Microscopic slides containing chromosomes at diakinesis stage were immunostained with α -MLH1 antibody as described (35). For immunostaining of γ H2AX, ASY1, H2A.W6, H2A.W7, and H3K9me2, fresh inflorescences were dissected and chromosomes spread were performed with lipsol. Immunostaining was performed as described (35).

GBS to Map Crossovers Genome-Wide. DNA was extracted from rosette leaves using the CTAB-based extraction procedure. DNA libraries were prepared as described (46) and sequenced on an Illumina NextSeq500 instrument. Sequencing reads (47) were mapped to the TAIR10 Col genome assembly using Bowtie 2 and crossover positions were identified using the TIGER pipeline as described (26, 48).

Chromatin Immunoprecipitation and MNase Analysis of Nucleosome Occupancy. ChIP and MNase were performed as described (49). To perform ChIP, 2 g of floral buds and 10 μ g of H2A.W7 antibody were used. For qPCR amplification, 0.25 ng of DNA and 0.7 μ M of primers were used with a QuantiNova SYBR Green PCR kit and a CFX96 qPCR instrument.

Generation of *h2a.w7:H2A.W7* and *h2a.w7:H2A.W7-S136A*. The full-length sequence of H2A.W7 including 819 bp of the upstream promoter sequence was amplified by PCR using the oligonucleotides H2A.W7.1 and H2A.W7.2 and cloned into pZP211 vector. To generate *h2a.w7:H2A.W7-S136A*, oligonucleotides H2A.W7.3 and H2A.W7.4 were used to amplify H2A.W7 and incorporate a point mutation T→G at position 707 using the Quick-change II site-directed mutagenesis kit (Agilent). *Arabidopsis* plants were transformed by the floral dipping method.

Pollen Typing. Pollen grains were isolated from hybrid F₁ plants and genomic DNA extracted as described (41). Using allele-specific oligonucleotides, PCR was performed to detect nonrecombinant and recombinant molecules. DNA extracted from leaf tissue of hybrid F₁ plants was used as negative control during the detection of recombinant molecules. Serial dilution of pollen DNA was used for PCR to determine the concentration of parental and recombinant molecules for each sample and the recombination rate was calculated as described (41).

RNA Sequencing. 100 mg of unopened floral buds was ground in liquid nitrogen and RNA was extracted using TRIzol reagent. RNA was treated with the Ribo-Zero rRNA Removal kit to deplete rRNA and the ScriptSeq v2 RNA-seq Library Preparation Kit (SSV21124, Epicentre) was used to make libraries. Sequencing reads (50) were mapped to the TAIR10 reference transcriptome using Salmon version 0.9.1 and differentially expressed transposons were identified as described (45).

Whole Genome Bisulfite Sequencing. DNA was extracted from unopened floral buds using the DNeasy Plant Pro Kit (Qiagen). Whole genome bisulfite sequencing libraries were generated as described (38) and sequenced (51) on a DNBSEQ sequencing platform.

Data, Materials, and Software Availability. All study data are included in the article and/or supporting information. Previously published data were used for this work (10, 29, 32, 45). Sequencing data for *h2a.w7* ColxLer GBS libraries have been deposited under ArrayExpress accession E-MTAB-15040, RNA-sequencing data for wild type, *cmt3*, *h2a.w7*, and *h2a.w7 cmt3* have been deposited under ArrayExpress accession E-MTAB-14268, and Whole Genome Bisulfite Sequencing

data of wild type, *h2a.w7*, *HP3*, and *h2a.w7 HP3* have been deposited under NCBI GEO accession [GSE291433](https://www.ncbi.nlm.nih.gov/geo/accession/GSE291433).

ACKNOWLEDGMENTS. We acknowledge the Gurdon institute for access to the imaging facilities, Carlos Poveda and Marie Lewis for access to the University of Reading flow cytometry facilities and assistance with instruments, Chris Franklin

for the ASY1 antibody, Mathilde Grelon for the MLH1 antibody, Frédéric Berger for the H2A.W6 and H2A.W7 antibodies, and Olivier Mathieu for *h2a.w6-2* and *h2a.w-2* seeds. Funding was provided by the Fundamental Research Funds for the Central Universities to Z.Z., European Research Council Grant ERC-2015-CoG-681987 "SynthHotSpot" to I.R.H., and by Biotechnology and Biological Sciences Research Council BB/Y001591/1 and BB/X011003/1 to C.L.

1. R. Mercier, C. Mézard, E. Jenczewski, N. Macaisne, M. Grelon, The molecular biology of meiosis in plants. *Annu. Rev. Plant Biol.* **66**, 297–327 (2015).
2. T. Robert *et al.*, The TopoVIB-Like protein family is required for meiotic DNA double-strand break formation. *Science*. **351**, 943–949 (2016).
3. N. Vrielynck *et al.*, A DNA topoisomerase VI-like complex initiates meiotic recombination. *Science*. **351**, 939–943 (2016).
4. A. G. Hinch *et al.*, The configuration of RPA, RAD51, and DMC1 binding in meiosis reveals the nature of critical recombination intermediates. *Mol. Cell*. **79**, 689–701 (2020).
5. D. K. Bishop, D. Park, L. Xu, N. Kleckner, DMC1: A meiosis-specific yeast homolog of E. coli recA required for recombination, synaptonemal complex formation, and cell cycle progression. *Cell*. **69**, 439–456 (1992).
6. M. G. Sehorn, S. Sigurdsson, W. Bussen, V. M. Unger, P. Sung, Human meiotic recombinase Dmc1 promotes ATP-dependent homologous DNA strand exchange. *Nature*. **429**, 433–437 (2004).
7. V. Cloud, Y. L. Chan, J. Grubb, B. Budke, D. K. Bishop, Rad51 is an accessory factor for Dmc1-mediated joint molecule formation during meiosis. *Science*. **337**, 1222–1225 (2012).
8. K. Choi, I. R. Henderson, Meiotic recombination hotspots—a comparative view. *Plant J.* **83**, 52–61 (2015).
9. A. J. Tock, I. R. Henderson, Hotspots for initiation of meiotic recombination. *Front. Genet.* **9**, 521 (2018).
10. K. Choi *et al.*, Nucleosomes and DNA methylation shape meiotic DSB frequency in *Arabidopsis thaliana* transposons and gene regulatory regions. *Genome Res.* **28**, 532–546 (2018).
11. C. J. Underwood *et al.*, Epigenetic activation of meiotic recombination near *Arabidopsis thaliana* centromeres via loss of H3K9me2 and non-CG DNA methylation. *Genome Res.* **28**, 519–531 (2018).
12. J. B. Fernandes *et al.*, Structural variation and DNA methylation shape the centromere-proximal meiotic crossover landscape in *Arabidopsis*. *Genome Biol.* **25**, 30 (2024).
13. N. E. Yelina *et al.*, DNA methylation epigenetically silences crossover hot spots and controls chromosomal domains of meiotic recombination in *Arabidopsis*. *Genes Dev.* **29**, 2183–2202 (2015).
14. K. Luger, M. L. Dechassa, D. J. Tremethick, New insights into nucleosome and chromatin structure: an ordered state or a disordered affair? *Nat. Rev. Mol. Cell Biol.* **13**, 436–447 (2012).
15. K. Luger, A. W. Mäder, R. K. Richmond, D. F. Sargent, T. J. Richmond, Crystal structure of the nucleosome core particle at 2.8 Å resolution. *Nature*. **389**, 251–260 (1997).
16. A. R. Cutter, J. J. Hayes, A brief review of nucleosome structure. *FEBS Lett.* **589**, 2914–2922 (2015).
17. C. M. Weber, S. Henikoff, Histone variants: Dynamic punctuation in transcription. *Genes Dev.* **28**, 672–682 (2014).
18. P. B. Talbert *et al.*, A unified phylogeny-based nomenclature for histone variants. *Epigenetics Chromatin*. **5**, 7 (2012).
19. T. Kawashima *et al.*, Diversification of histone H2A variants during plant evolution. *Trends Plant Sci.* **20**, 419–425 (2015).
20. A. Osakabe *et al.*, Histone H2A variants confer specific properties to nucleosomes and impact on chromatin accessibility. *Nucleic Acids Res.* **46**, 7675–7685 (2018).
21. B. Lei *et al.*, A synthetic approach to reconstruct the evolutionary and functional innovations of the plant histone variant H2A.W. *Curr. Biol.* **31**, 182–191 (2021).
22. R. Yelagandula *et al.*, The histone variant H2A.W defines heterochromatin and promotes chromatin condensation in *Arabidopsis*. *Cell*. **158**, 98–109 (2014).
23. Z. J. Lorković *et al.*, Compartmentalization of DNA damage response between heterochromatin and euchromatin is mediated by distinct H2A histone variants. *Curr. Biol.* **27**, 1192–1199 (2017).
24. E. Roitinger *et al.*, Quantitative phosphoproteomics of the ataxia telangiectasia-mutated (ATM) and ataxia telangiectasia-mutated and rad3-related (ATR) dependent DNA damage response in *Arabidopsis thaliana*. *Mol. Cell. Proteomics*. **14**, 556–571 (2015).
25. S. J. Armstrong, A. P. Caryl, G. H. Jones, F. C. Franklin, Asy1, a protein required for meiotic chromosome synapsis, localizes to axis-associated chromatin in *Arabidopsis* and *Brassica*. *J. Cell Sci.* **115**, 3645–3655 (2002).
26. H. Serra *et al.*, Massive crossover elevation via combination of HEI10 and recq4a recq4b during *Arabidopsis* meiosis. *Proc. Natl. Acad. Sci. U.S.A.* **115**, 2437–2442 (2018).
27. K. E. Francis *et al.*, Pollen tetrad-based visual assay for meiotic recombination in *Arabidopsis*. *Proc. Natl. Acad. Sci. U.S.A.* **104**, 3913–3918 (2007).
28. N. E. Yelina *et al.*, Epigenetic remodeling of meiotic crossover frequency in *Arabidopsis thaliana* DNA methyltransferase mutants. *PLoS Genet.* **8**, e1002844 (2012).
29. N. E. Yelina *et al.*, High-throughput analysis of meiotic crossover frequency and interference via flow cytometry of fluorescent pollen in *Arabidopsis thaliana*. *Nat. Protoc.* **8**, 2119–2134 (2013).
30. C. Melamed-Bessudo, E. Yehuda, A. R. Stuitje, A. A. Levy, A new seed-based assay for meiotic recombination in *Arabidopsis thaliana*. *Plant J.* **43**, 458–466 (2005).
31. O. Da Ines, K. Abe, C. Goubely, M. E. Gallego, C. I. White, Differing requirements for RAD51 and DMC1 in meiotic pairing of centromeres and chromosome arms in *Arabidopsis thaliana*. *PLoS Genet.* **8**, e1002636 (2012).
32. L. Chelysheva *et al.*, An easy protocol for studying chromatin and recombination protein dynamics during *Arabidopsis thaliana* meiosis: Immunodetection of cohesins, histones and MLH1. *Cytogenet Genome Res.* **129**, 143–153 (2010).
33. L. Giraut *et al.*, Genome-wide crossover distribution in *Arabidopsis thaliana* meiosis reveals sex-specific patterns along chromosomes. *PLoS Genet.* **7**, e1002354 (2011).
34. C. Morgan *et al.*, Diffusion-mediated HEI10 coarsening can explain meiotic crossover positioning in *Arabidopsis*. *Nat. Commun.* **12**, 4674 (2021).
35. C. Lambing, P. C. Kuo, A. J. Tock, S. D. Topp, I. R. Henderson, ASY1 acts as a dosage-dependent antagonist of telomere-led recombination and mediates crossover interference in *Arabidopsis*. *Proc. Natl. Acad. Sci. U.S.A.* **117**, 13647–13658 (2020).
36. J. Du *et al.*, Dual binding of chromomethylase domains to H3K9me2-containing nucleosomes directs DNA methylation in plants. *Cell*. **151**, 167–180 (2012).
37. P. Bourguet *et al.*, The histone variant H2A.W and linker histone H1 co-regulate heterochromatin accessibility and DNA methylation. *Nat. Commun.* **12**, 2683 (2021).
38. C. J. Harris, Z. Zhong, L. Ichino, S. Feng, S. E. Jacobsen, H1 restricts euchromatin-associated methylation pathways from heterochromatic encroachment. *eLife* **12**, RP89353 (2024).
39. K. Rutowicz *et al.*, A specialized histone H1 variant is required for adaptive responses to complex abiotic stress and related DNA methylation in *Arabidopsis*. *Plant Physiol.* **169**, 2080–2101 (2015).
40. J. Walker *et al.*, Sexual-lineage-specific DNA methylation regulates meiosis in *Arabidopsis*. *Nat. Genet.* **50**, 130–137 (2018).
41. K. Choi, N. E. Yelina, H. Serra, I. R. Henderson, Quantification and sequencing of crossover recombinant molecules from *Arabidopsis* pollen DNA. *Methods Mol. Biol.* **1551**, 23–57 (2017).
42. T. Fan *et al.*, *Arabidopsis* γ-H2A.X-INTERACTING PROTEIN participates in DNA damage response and safeguards chromatin stability. *Nat. Commun.* **13**, 7942 (2022).
43. O. Da Ines *et al.*, Meiotic recombination in *Arabidopsis* is catalysed by DMC1, with RAD51 playing a supporting role. *PLoS Genet.* **9**, e1003787 (2013).
44. P. A. Ziolkowski *et al.*, Juxtaposition of heterozygous and homozygous regions causes reciprocal crossover remodelling via interference during *Arabidopsis* meiosis. *eLife* **4**, e03708 (2015).
45. E. J. Lawrence *et al.*, Natural variation in TBP-associated factor 4b controls meiotic crossover and germline transcription in *Arabidopsis*. *Curr. Biol.* **29**, 2676–2686 (2019).
46. P. Kuo, I. R. Henderson, C. Lambing, CTAB DNA extraction and genotyping-by-sequencing to map meiotic crossovers in plants. *Methods Mol. Biol.* **2484**, 43–53 (2022).
47. C. Lambing, Identifying crossover locations in *Arabidopsis thaliana* h2a.w7 Col-0 × Ler F2 populations using genotyping-by-sequencing, ArrayExpress E-MTAB-15040. BioStudies. <https://www.ebi.ac.uk/biostudies/arrayexpress>. Deposited 10 April 2025.
48. B. A. Rowan, V. Patel, D. Weigel, K. Schneeberger, Rapid and inexpensive whole-genome genotyping-by-sequencing for crossover localization and fine-scale genetic mapping. *G3*, **5**, 385–398 (2015).
49. C. Lambing, K. Choi, A. R. Blackwell, I. R. Henderson, Chromatin Immunoprecipitation of meiotically expressed proteins from *Arabidopsis thaliana* flowers. *Methods Mol. Biol.* **2061**, 219–236 (2020).
50. C. Lambing, RNA-seq of Col, h2a.w7, cmt3 and h2a.w7 cmt3 *Arabidopsis thaliana* floral buds, ArrayExpress E-MTAB-14268. BioStudies. <https://www.ebi.ac.uk/biostudies/arrayexpress>. Deposited 22 July 2024.
51. Z. Zhong, Whole genome bisulfite sequencing of Col, h2a.w7, HP3 and h2a.w7 x HP3 *Arabidopsis thaliana* floral buds, NCBI GSE291433. GEO. <https://www.ncbi.nlm.nih.gov/geo/>. Deposited 3 August 2024.